doi:10.1093/brain/awx293 BRAIN 2018: 141; 302–317 | 302

BRAIN
A JOURNAL OF NEUROLOGY

Longitudinal structural and molecular neuroimaging in agrammatic primary progressive aphasia

Katerina A. Tetzloff,[1] Joseph R. Duffy,[2] Heather M. Clark,[2] Edythe A. Strand,[2] Mary M. Machulda,[3] Christopher G. Schwarz,[1] Matthew L. Senjem,[1,4] Robert I. Reid,[1,3] Anthony J. Spychalla,[1] Nirubol Tosakulwong,[5] Val J. Lowe,[1] Clifford R. Jack, Jr,[1] Keith A. Josephs[2] and Jennifer L. Whitwell[1]

The agrammatic variant of primary progressive aphasia affects normal grammatical language production, often occurs with apraxia of speech, and is associated with left frontal abnormalities on cross-sectional neuroimaging studies. We aimed to perform a detailed assessment of longitudinal change on structural and molecular neuroimaging to provide a complete picture of neurodegeneration in these patients, and to determine how patterns of progression compare to patients with isolated apraxia of speech (primary progressive apraxia of speech). We assessed longitudinal structural MRI, diffusion tensor imaging and ^{18}F-fluorodeoxyglucose PET in 11 agrammatic aphasia subjects, 20 primary progressive apraxia of speech subjects, and 62 age and gender-matched controls with two serial assessments. Rates of change in grey matter volume and hypometabolism, and white matter fractional anisotropy, mean diffusivity, radial diffusivity and axial diffusivity were assessed at the voxel-level and for numerous regions of interest. The greatest rates of grey matter atrophy in agrammatic aphasia were observed in inferior, middle, and superior frontal gyri, premotor and motor cortices, as well as medial temporal lobe, insula, basal ganglia, and brainstem compared to controls. Longitudinal decline in metabolism was observed in the same regions, with additional findings in medial and lateral parietal lobe. Diffusion tensor imaging changes were prominent bilaterally in inferior and middle frontal white matter and superior longitudinal fasciculus, as well as right inferior fronto-occipital fasciculus, superior frontal and precentral white matter. More focal patterns of degeneration of motor and premotor cortex were observed in primary progressive apraxia of speech. Agrammatic aphasia showed greater rates of grey matter atrophy, decline in metabolism, and white matter degeneration compared to primary progressive apraxia of speech in the left frontal lobe, predominantly inferior and middle frontal grey and white matter. Correlations were also assessed between rates of change on neuroimaging and rates of clinical decline. Progression of aphasia correlated with rates of degeneration in frontal and temporal regions within the language network, while progression of parkinsonism and limb apraxia correlated with degeneration of motor cortex and brainstem. These findings demonstrate that disease progression in agrammatic aphasia is associated with widespread neurodegeneration throughout regions of the language network, as well as connecting white matter tracts, but also with progression to regions outside of the language network that are responsible for the development of motor symptoms. The fact that patterns of progression differed from primary progressive apraxia of speech supports the clinical distinction of these syndromes.

1 Department of Radiology, Mayo Clinic, Rochester, MN, USA
2 Department of Neurology, Mayo Clinic, Rochester, MN, USA
3 Department of Psychology and Psychiatry, Mayo Clinic, Rochester, MN, USA
4 Department of Information Technology, Mayo Clinic, Rochester, MN, USA
5 Department of Health Sciences Research (Biostatistics), Mayo Clinic, Rochester, MN, USA

Received August 17, 2016. Revised April 11, 2017. Accepted September 20, 2017. Advance Access publication December 8, 2017

Correspondence to: Jennifer L. Whitwell, PhD
Associate Professor of Radiology
Mayo Clinic
200 1st St SW, Rochester, MN 55905
USA
E-mail: Whitwell.jennifer@mayo.edu

Keywords: apraxia of speech; rates; magnetic resonance imaging; diffusion tensor imaging; FDG-PET

Abbreviations: agPPA = agrammatic variant of primary progressive aphasia; AOS = apraxia of speech; DTI = diffusion tensor imaging; FDG = fluorodeoxyglucose; PPA = primary progressive aphasia; PPAOS = primary progressive apraxia of speech; WAB-AQ = Western Aphasia Battery-Aphasia Quotient

Introduction

Primary progressive aphasia (PPA) is a neurodegenerative disease in which language deficits are the primary and most salient feature, while other aspects of cognition are left relatively unaffected (Mesulam, 1982). Of main interest in this study is the agrammatic variant of PPA (agPPA), which is clinically characterized by agrammatic or telegraphic speech (Gorno-Tempini *et al.*, 2011; Botha *et al.*, 2015). These deficits may include, for example, omitting functional morphemes, producing words in the wrong order, simplifying grammatical forms and sentences, and speaking at a reduced rate. Furthermore, agPPA often presents concomitantly with apraxia of speech (AOS) (Duffy, 2005; Josephs *et al.*, 2013; Duffy *et al.*, 2014), resulting in articulatory errors and distortions, as well as motorically slow speaking rate (Jung *et al.*, 2013).

Cross-sectional studies have associated agPPA with significant grey matter loss on MRI and hypometabolism on FDG-PET in the left frontal lobe, including Broca's area, precentral gyrus, insula, and temporal lobe (Josephs *et al.*, 2006, 2013; Peelle *et al.*, 2008; Galantucci *et al.*, 2011; Rogalski *et al.*, 2011, 2014; Mesulam, 2013; Brambati *et al.*, 2015). White matter tract degeneration measured using diffusion tensor imaging (DTI) has also been noted in the superior longitudinal fasciculus (Whitwell *et al.*, 2010; Galantucci *et al.*, 2011; Brambati *et al.*, 2015). These cross-sectional neuroanatomical abnormalities have also been shown to be associated with the speech and language features observed in agPPA subjects (Amici *et al.*, 2007; Peelle *et al.*, 2008; Whitwell *et al.*, 2013*a*). Despite these robust cross-sectional neuroimaging data, longitudinal imaging studies have received less attention within the agPPA population. A couple of groups have reported on regional volume changes over time in agPPA (Rogalski *et al.*, 2014; Mandelli *et al.*, 2016) and one has reported changes over time in DTI measures (Lam *et al.*, 2014). However, longitudinal changes on FDG-PET have not been assessed and these different neuroimaging modalities have not been investigated concurrently in the same cohort and so it is unclear how they compare as potential disease biomarkers. In addition, no study has assessed correlations between neuroanatomical data and clinical measures using longitudinal data in agPPA.

While patients with agPPA can present with both agrammatism and AOS, it has been recognized that AOS can be the sole or dominant manifestation of neurodegeneration. This isolated variant, termed primary progressive AOS (PPAOS), is characterized by slow speech rate, articulatory distortions and groping, distorted sound substitutions, and syllable segmentation (Josephs *et al.*, 2006, 2012; Jung *et al.*, 2013). Unlike in agPPA, aphasia is absent early in the disease course. Cross-sectional neuroimaging analyses have demonstrated that PPAOS subjects have relatively focal grey matter loss bilaterally in lateral and medial premotor regions, with white matter degeneration found not only in these regions but also in the superior longitudinal fasciculus (Josephs *et al.*, 2006, 2008*b*, 2012, 2014; Whitwell *et al.*, 2013*a*). This pattern differs from agPPA, with agPPA showing more widespread involvement of the frontal and temporal lobes (Josephs *et al.*, 2013). Longitudinal neuroimaging has been described in PPAOS, with grey matter atrophy spreading from the initial focal premotor pattern into the prefrontal and motor cortices, in addition to the basal ganglia and midbrain (Josephs *et al.*, 2014; Whitwell *et al.*, 2017). However, it is unknown how these longitudinal patterns of atrophy compare to those observed in agPPA, and whether the syndromes remain relatively distinct on neuroimaging as the diseases progress or whether they converge into similar patterns of progression, especially given that PPAOS subjects can develop agrammatism over time (Josephs *et al.*, 2014; Whitwell *et al.*, 2017).

The purpose of this study was, therefore, to comprehensively characterize disease progression in agPPA by assessing longitudinal patterns of structural and molecular change in the brain and determine whether these patterns differ from those observed in PPAOS. In addition, in order to shed light on the neuroanatomical underpinnings of clinical disease progression, we aimed to examine correlations between regional patterns of longitudinal brain change and progression of clinical symptoms over the same time interval. In this multimodality neuroimaging study, we assessed rates of atrophy in grey matter using structural MRI, white matter using DTI and hypometabolism using FDG-PET.

Materials and methods

Subjects

Eleven subjects fulfilling diagnostic criteria for agPPA (Gorno-Tempini *et al.*, 2011; Botha *et al.*, 2015) and 20 subjects fulfilling diagnostic criteria for PPAOS (Josephs *et al.*, 2012) underwent two serial MRIs with an interval of ~1.5 years. Subjects were originally recruited into a cross-sectional NIH grant and were diagnosed with either agPPA or PPAOS at their baseline research visit based on performance in an extensive speech and language evaluation in the Department of Neurology at the Mayo Clinic. Subjects were diagnosed with agPPA if agrammatism was present in the speech or writing samples and was the sole or dominant presenting sign; if AOS was also present, which it was in six subjects, it was unequivocally equal to or less severe than the agrammatism. A designation of agrammatism was made if the speech or writing sample included two or more instances of function word omission, errors in word order, or inappropriate morphology (e.g. verb tense). Subjects were diagnosed with PPAOS if the predominant deficit was AOS and other neurological and aphasic traits were absent or no more than equivocal. These diagnoses were made after the review of video and audio recordings and the scores of the speech and language tests, which are described below, by two speech-language pathologists. None of the subjects met criteria for semantic or logopenic PPA (Gorno-Tempini *et al.*, 2011). These subjects returned for follow-up examinations as a part of another NIH-funded longitudinal grant, during which the same neurological and speech and language evaluations were performed.

These 31 subjects were matched 2:1 to 62 healthy controls by age, gender, and scan interval. The controls had been recruited for the Mayo Clinic Study of Aging (Roberts *et al.*, 2008; Petersen *et al.*, 2010). The healthy controls had a median [interquartile range (IQR)] age at baseline of 69 (63, 75) years and consisted of 55% females, with a median (IQR) scan interval in years of 1.6 (1.2, 2.3).

Speech and language battery

The battery included the Western Aphasia Battery (WAB) (Kertesz, 2007), Part 1; this test measures global language ability, including lexical content, fluency, repetition, naming, and spoken language comprehension sub-scores, which are then combined to form an overall WAB Aphasia Quotient (WAB-AQ). The Token Test, Part V (De Renzi and Vignolo, 1962) was used to further measure verbal syntactic comprehension, and the 15-item Boston Naming Test (Lansing *et al.*, 1999) was used to measure subjects' ability at confrontation-naming. Judgements about motor speech abilities were based on spoken language tasks of the WAB plus additional speech tasks that included vowel prolongation, speech alternating motion rates, speech sequential motion rates, word and sentence repetition, and a conversational speech sample. The severity of motor speech impairment (including AOS and dysarthria) was rated using a minimally adapted version of the Motor Speech Disorders (MSD) scale (Yorkston *et al.*, 1993), and the severity of AOS was specifically measured using the AOS rating scale (ASRS) (Strand *et al.*, 2014). The Northwestern Anagram Test (NAT) (Weintraub *et al.*, 2009), which assessed syntactic production without requiring speech, was performed only at the second examination.

Neurological battery

All subjects also underwent a neurological examination by a behavioural neurologist (K.A.J.). The neurological battery included assessing general cognitive function with the Montreal Cognitive Assessment Battery (MoCA) (Nasreddine *et al.*, 2005), executive function with the Frontal Assessment Battery (FAB) (Dubois *et al.*, 2000), praxis with the limb apraxia subscale of the WAB (Kaufer *et al.*, 2000), functional performance with the Clinical Dementia Rating Scale sum of boxes (CDR-SB) (Hughes *et al.*, 1982), neuropsychiatric features with the brief questionnaire from the Neuropsychiatric Inventory (NPI-Q) (Kaufer *et al.*, 2000), and motor function with the Movement Disorders Society sponsored revision of the Unified Parkinson's Disease Rating Scale (MDS-UPDRS) Part III (Goetz *et al.*, 2008).

Image acquisition

All subjects underwent a standardized MRI protocol at 3.0 T at both time points, which included a 3D magnetization prepared rapid acquisition gradient echo (MPRAGE) sequence and a single-shot echo-planar DTI pulse sequence with 41 diffusion encoding directions, as previously described (Josephs *et al.*, 2012). All subjects also underwent FDG-PET at both time-points using a PET/CT scanner (GE Healthcare) operating in 3D mode. Subjects were injected with approximately 459 MBq of FDG (range 367–576 MBq) and PET acquisition occurred after a 30-min uptake period. All subjects also underwent a Pittsburgh compound B (PiB) PET scan at baseline, and a global PiB standardized uptake value ratio (SUVR) was calculated as previously described (Jack *et al.*, 2008).

Structural MRI

Longitudinal patterns of atrophy were assessed using an in-house developed version of tensor-based morphometry using symmetric normalization (TBM-SyN) (Jack *et al.*, 2014; Cash *et al.*, 2015), using Advanced Normalization Tools (ANTs) software (http://picsl.upenn.edu/software/ants) and Statistical Parametric Mapping (SPM5) (www.fil.ion.ucl.ac.uk/spm) software. The symmetric normalization (SyN) algorithm (Avants *et al.*, 2008) from ANTs forces the deformation between two MPRAGE images to be symmetric with respect to the direction of the deformation, eliminating asymmetry in the registrations and ensuring that the absolute changes from scan A–B are the same as from B–A. Prior to computing SyN deformations, all serial scans for each subject were co-registered using a 9DOF linear registration to their common mean and an in-house developed implementation of differential bias correction was run on each subject's scans in order to remove intensity inhomogeneity bias, in a manner similar to that of Lewis and Fox (2004). ANTs software was then used to compute a SyN deformation between each scan pair. The SyN algorithm was used to compute a non-linear deformation required to transform the later image to the earlier image for each pair of scans, producing an image of the log of the Jacobian determinants for

each. These log Jacobian images were then scaled by the inter-scan interval in years, thus producing annualized log Jacobian images. The SyN deformation was applied to warp the late image to the early image, and the warped late image was then averaged with the early image to form a softmean image in the space of the early image. We applied unified segmentation (Ashburner and Friston, 2005), with a custom elderly template (Vemuri *et al.*, 2008) to each softmean image, and used the resulting spatial normalization parameters to propagate the annualized log Jacobian images to template space. The spatially normalized annualized log Jacobian images were smoothed at 10 mm full-width at half-maximum (FWHM) and entered into an SPM design matrix for statistical analysis. Region of interest level rates of atrophy were also calculated from the log Jacobian images using the automated anatomical labelling (AAL) atlas (Tzourio-Mazoyer *et al.*, 2002).

Diffusion tensor imaging

Each volume of the DTI image was registered to the first volume (a b0) using affine transformations to correct for head motion and minimize distortions due to eddy currents. Images were brain-extracted, and fractional anisotropy, mean diffusivity, radial diffusivity, and axial diffusivity were generated using weighted least-squares optimization with Dipy (Garyfallidis *et al.*, 2014).

Longitudinal patterns of white matter degeneration were estimated. In brief, for each DTI metric (fractional anisotropy, mean diffusivity, radial diffusivity, axial diffusivity) the ANTs SyN algorithm (Avants *et al.*, 2008) was used to compute deformation fields between baseline and follow-up pair images in both directions (baseline to follow-up and follow-up to baseline). Non-linear deformation calculations were performed in a halfway-space of the affine alignment between the two time-points, decreasing bias (Yushkevich *et al.*, 2010). Annualized log Jacobian values were computed from each deformation field. For voxel-wise comparison, these were warped to the FMRIB58_FA_1 mm standard template space (http://fsl.fmrib.ox.ac.uk/fsl/fslwiki/FMRIB58_FA) using ANTs transformations computed between each time-point's DTI fractional anisotropy images and the (DTI fractional anisotropy-weighted) template. The template-space annualized log-Jacobian values were then averaged across the two computation directions (after inverting the backwards direction), and smoothed at 10 mm FWHM. Voxels with fractional anisotropy <0.2 (non-white matter voxels) were omitted. For region of interest-based comparisons, the Johns Hopkins University (JHU) single-subject white matter atlas (Oishi *et al.*, 2009) was applied using ANTs warps to estimate the mean of the annualized log-Jacobian values within each region of interest, omitting voxels with fractional anisotropy <0.2 (non-white matter voxels).

FDG-PET

For each subject, at each time point, we first co-registered the FDG-PET image to the corresponding MPRAGE, used the unified segmentation algorithm in SPM (Ashburner and Friston, 2005) to determine a spatial normalization mapping between the MPRAGE and our custom elderly template. We applied the resulting template-to-subject mapping to the AAL atlas. Median FDG-PET uptake value was then calculated for the pons, and every voxel in the FDG-PET was divided by this value, to obtain an FDG-PET standardized uptake value ratio (SUVR) image. For a parallel analysis using partial volume correction (Meltzer *et al.*, 1990), we used the grey and white matter segmentations of the MRI scan to form a brain mask, binarized and smoothed the mask with a 6 mm FWHM Gaussian kernel, then divided the FDG-PET SUVR image by this mask at each voxel. Next, we applied the subject-to-template mapping to the FDG-PET SUVR image at each time point, and subtracted the resulting spatially normalized images (baseline minus follow-up), to obtain a spatially normalized image of FDG-PET decrease over time in each subject. We smoothed the resulting FDG serial change images with an 8 mm FWHM Gaussian smoothing kernel prior to entering them into statistical analysis. Region of interest level rates of decline in metabolism were also calculated using the AAL atlas (Tzourio-Mazoyer *et al.*, 2002).

Statistics

Voxel-level statistical analysis of the grey matter volume, fractional anisotropy, mean diffusivity, radial diffusivity and axial diffusivity Jacobians, and FDG-PET change images, were performed in SPM using multiple regression analyses. Results were assessed after correction for multiple comparisons using the false discovery rate (FDR) correction at $P < 0.01$. In addition, multiple regression analyses were used to assess correlations between annualized log Jacobians and annualized rates of change in clinical scores. We assessed clinical scores that represented the main clinical domains that change over time in these patients, i.e. aphasia (WAB-AQ), AOS (ASRS), parkinsonism (MDS-UPDRS part III) and limb apraxia (WAB-apraxia). Given that no differences were observed between agPPA and PPAOS in change over time on ASRS, MDS-UPDRS part III or WAB-apraxia, the regression analyses for these variables were performed using all agPPA and PPAOS subjects. Since aphasia was only present in the agPPA group at baseline, the regression analyses for WAB-AQ were performed using all agPPA and PPAOS subjects to provide maximum power and were also repeated using only the agPPA subjects. Given that these are exploratory analyses, results were assessed uncorrected for multiple comparisons at $P < 0.001$, as well as with the FDR correction at $P < 0.01$.

The statistical analyses of region of interest level data were performed using RStudio 0.99.902 (Team R, 2015). Inter-group comparisons were performed using Mann-Whitney U-tests and all *P*-values were reported after correction for multiple comparisons using the FDR correction. Group differences were summarized with the area under the receiver operating characteristic curve (AUROC). The AUROC is a non-parametric effect size estimate that does not depend on the scale of the measurement and hence allows a comparison of the strength of group discrimination across different neuroimaging metrics (Acion *et al.*, 2006). Additionally, annualized rates of change were calculated for the clinical variables and all clinical and demographic variables were compared using two-sided *t*-tests for continuous variables or chi-squared tests for categorical variables.

Table 1 Demographics and clinical scores

		agPPA	PPAOS	*P*-value
Demographics				
Gender (% female)		62.5	45	0.43
Age at exam in years		68.65 (65, 72.95)	71 (64.55, 76.1)	0.51
Age at onset in years		66.5 (60, 71.38)	67.5 (60.75, 73)	0.83
Disease duration in years		1.75 (1, 2.5)	3.25 (2.375, 4.812)	0.05
Scan interval in years		1.46 (1.15, 1.60)	1.80 (1.45, 2.52)	0.01
Global PiB SUVR		1.27 (1.20, 1.39)	1.24 (1.21, 1.30)	0.50
Speech and language variables				
WAB-AQ (/100, 100 = best)	Base	84.4 (82.53, 90.05)	97.5 (95.9, 99.8)	<0.0001
	Rate	−9.83 (−13.11, −8.04)	−1.33 (−3.85, −0.15)	0.002
Token Test (/22, 22 = best)	Base	13 (6.75, 17.25)	21 (20, 22)	<0.0001
	Rate	−3.49 (−6.19, −2.94)	−0.62 (−1.25, 0)	0.0004
BNT (/15, 15 = best)	Base	14 (13.24, 15)	15 (13.75, 15)	0.13
	Rate	−1.84 (−3.48, −1.37)	0 (−0.57, 0)	0.05
ASRS (/64, 0 = best)	Base	6 (1, 9.25)	16.5 (13.5, 21.25)	<0.0001
	Rate	1.48 (0.17, 4.97)	4.23 (1.48, 5.81)	0.87
MSD (/10, 10 = best)	Base	9.5 (7.75, 10)	7 (6.75, 8)	<0.0001
	Rate	−0.12 (−1.56, −0.23)	−0.77 (−1.27, −0.48)	0.60
NAT (/10, 10 = best)	Repeat	3 (2, 4.75)	9 (6.5, 9.5)	0.009
Neurological variables				
MoCA (/30, 30 = best)	Base	24 (23.5, 24)	28 (25, 29)	<0.0001
	Rate	−4.48 (−8.19 −2.01)	−0.17 (−1.22, 0)	0.003
Limb apraxia (/60, 60 = best)	Base	56 (47, 57.50)	58(77, 59.25)	0.05
	Rate	−4.60 (−7.69, −3.09)	−1.55 (−3.58, −0.39)	0.11
UPDRS-III (/132, 0 = best)	Base	11 (9.5, 19)	8 (5, 14.25)	0.39
	Rate	14.84 (−0.52, 19.23)	5.18 (0.97, 14.64)	0.42
FAB /(18, best = 18)	Base	13 (11, 16)	17 (16, 17.25)	0.006
	Rate	−1.75 (−3.89, −0.90)	−1.09 (−1.26, −0.30)	0.13
CDR-SB (/18, 0 = best)	Base	1 (0.25, 2)	0 (0, 0)	0.04
	Rate	0.67 (0.12, 6.55)	0 (0, 0.58)	0.04
NPI-Q (/36, 0 = best)	Base	2 (0, 2)	1.5 (0.75, 4)	0.20
	Rate	1.23 (0, 2.41)	0 (−0.04, 0.46)	0.03

Results are shown as median (IQR). Baseline values and annualized rates of change (points per year) are given for each speech and language and neurological variable. Note that the NAT data were collected at the repeat assessment only.

ASRS = Apraxia of Speech Rating Scale; BNT = Boston Naming Test; CDR = Clinical Dementia Rating Scale sum of boxes; FAB = Frontal Assessment Battery; MoCA = Montreal Cognitive Assessment Battery; MSD = Motor Speech Disorder scale; NAT = Northwestern Anagram Test; NPI-Q = Neuropsychiatric Inventory; PiB SUVR = Pittsburgh Compound B standardized uptake value ratio; UPDRS-III = Unified Parkinson's Disease Rating Scale Part III.

Results

Demographic and clinical features

There were no significant differences between agPPA and PPAOS in gender, age of disease onset, and disease duration at baseline (Table 1). The median scan interval was slightly shorter in agPPA (1.5 years) compared to PPAOS (1.8 years, $P = 0.01$). The majority of all agPPA and PPAOS subjects were PiB-negative (SUVR < 1.50) (91% and 90%). The agPPA subjects performed worse on the MoCA, WAB-AQ, and the Token Test, but better on the ASRS and the MSD compared to PPAOS at baseline, who, as expected, performed normally on all of the language measures. The agPPA subjects had significantly higher rates of decline than the PPAOS subjects for MoCA, WAB-AQ, Token Test, CDR-SB, and NPI-Q (Table 1).

Structural MRI

When comparing agPPA subjects to controls at the region of interest level (Table 2), increased rates of grey matter atrophy were observed throughout dorsolateral and medial frontal lobe, as well as premotor and motor cortices. Rates of atrophy were increased in both hemispheres but greater in the left hemisphere. Increased rates were also observed bilaterally in middle cingulate cortex, medial temporal lobe, left insula and striatum. The voxel-based analysis also showed greater atrophy rates throughout the frontal lobes, particularly in the left hemisphere, but also showed additional atrophy in the left superior lateral and medial temporal regions, the inferior and medial parietal lobes, and brainstem (Fig. 1).

PPAOS showed increased rates of grey matter atrophy compared to controls in similar regions at the region of interest level, although more robust findings were observed in the paracentral and postcentral cortices, and left

Table 2 Annualized rates of grey matter atrophy across regions of interest

Region of interest	Hem	Control	AgPPA	PPAOS	agPPA ~ Control	PPAOS ~ Control	agPPA ~ PPAOS
					AUROC (*P*)	AUROC (*P*)	AUROC (*P*)
Broca's area	L	−0.005 (0.01)	−0.048 (0.021)	−0.019 (0.014)	0.987 (<0.001)	0.816 (<0.001)	0.895 (0.006)
	R	−0.006 (0.008)	−0.025 (0.022)	−0.014 (0.018)	0.775 (0.01)	0.74 (0.004)	0.645 (0.532)
Middle frontal	L	−0.007 (0.012)	−0.042 (0.019)	−0.018 (0.015)	0.966 (<0.001)	0.713 (0.011)	0.841 (0.03)
	R	−0.007 (0.011)	−0.022 (0.025)	−0.013 (0.017)	0.763 (0.014)	0.639 (0.104)	0.636 (0.55)
Superior frontal	L	−0.008 (0.014)	−0.043 (0.02)	−0.021 (0.017)	0.937 (<0.001)	0.726 (0.007)	0.805 (0.043)
	R	−0.007 (0.014)	−0.03 (0.024)	−0.018 (0.019)	0.858 (0.001)	0.691 (0.023)	0.705 (0.302)
Superior medial frontal	L	−0.006 (0.015)	−0.039 (0.032)	−0.015 (0.015)	0.891 (<0.001)	0.684 (0.028)	0.741 (0.219)
	R	−0.007 (0.012)	−0.029 (0.027)	−0.014 (0.015)	0.779 (0.009)	0.629 (0.133)	0.691 (0.307)
Orbitofrontal cortex	L	−0.013 (0.022)	−0.025 (0.028)	−0.009 (0.013)	0.63 (0.215)	0.504 (0.961)	0.65 (0.525)
	R	−0.009 (0.013)	−0.012 (0.024)	−0.007 (0.01)	0.522 (0.864)	0.547 (0.573)	0.55 (0.888)
Anterior cingulate	L	−0.004 (0.014)	−0.017 (0.027)	−0.008 (0.014)	0.656 (0.144)	0.602 (0.238)	0.6 (0.687)
	R	−0.004 (0.012)	−0.014 (0.027)	−0.008 (0.013)	0.665 (0.126)	0.593 (0.273)	0.595 (0.687)
Middle cingulate	L	−0.002 (0.009)	−0.019 (0.015)	−0.011 (0.012)	0.838 (0.001)	0.749 (0.003)	0.659 (0.48)
	R	−0.004 (0.009)	−0.016 (0.015)	−0.007 (0.014)	0.83 (0.002)	0.659 (0.06)	0.691 (0.307)
Insula	L	−0.003 (0.009)	−0.029 (0.02)	−0.008 (0.01)	0.906 (<0.001)	0.675 (0.037)	0.823 (0.039)
	R	−0.004 (0.01)	−0.013 (0.022)	−0.005 (0.011)	0.689 (0.083)	0.563 (0.451)	0.641 (0.541)
Supplementary motor area	L	−0.004 (0.012)	−0.053 (0.021)	−0.038 (0.017)	0.972 (<0.001)	0.952 (<0.001)	0.709 (0.302)
	R	−0.005 (0.01)	−0.044 (0.027)	−0.03 (0.017)	0.902 (<0.001)	0.911 (<0.001)	0.709 (0.302)
Rolandic operculum	L	−0.004 (0.01)	−0.02 (0.021)	−0.014 (0.011)	0.802 (0.005)	0.79 (0.001)	0.614 (0.608)
	R	−0.004 (0.011)	−0.014 (0.017)	−0.013 (0.02)	0.745 (0.022)	0.803 (<0.001)	0.514 (0.94)
Precentral	L	−0.002 (0.01)	−0.045 (0.029)	−0.033 (0.013)	0.975 (<0.001)	0.956 (<0.001)	0.545 (0.888)
	R	−0.003 (0.01)	−0.03 (0.024)	−0.032 (0.018)	0.832 (0.002)	0.939 (<0.001)	0.505 (0.984)
Postcentral	L	−0.004 (0.008)	−0.011 (0.024)	−0.013 (0.013)	0.636 (0.197)	0.78 (0.001)	0.532 (0.888)
	R	−0.003 (0.011)	−0.007 (0.021)	−0.012 (0.019)	0.62 (0.248)	0.707 (0.013)	0.568 (0.824)
Paracentral lobule	L	−0.002 (0.01)	−0.017 (0.024)	−0.02 (0.014)	0.735 (0.029)	0.88 (<0.001)	0.55 (0.888)
	R	−0.004 (0.011)	−0.017 (0.022)	−0.017 (0.017)	0.684 (0.089)	0.764 (0.002)	0.541 (0.888)
Lateral temporal	L	−0.008 (0.01)	−0.025 (0.023)	−0.011 (0.011)	0.705 (0.059)	0.587 (0.292)	0.659 (0.48)
	R	−0.008 (0.01)	−0.012 (0.017)	−0.01 (0.012)	0.621 (0.248)	0.585 (0.296)	0.555 (0.888)
Medial temporal	L	−0.008 (0.009)	−0.034 (0.025)	−0.012 (0.01)	0.869 (0.001)	0.63 (0.131)	0.805 (0.043)
	R	−0.007 (0.01)	−0.016 (0.011)	−0.011 (0.008)	0.726 (0.036)	0.666 (0.05)	0.618 (0.595)
Lateral parietal	L	−0.007 (0.011)	−0.021 (0.022)	−0.013 (0.019)	0.678 (0.099)	0.643 (0.095)	0.586 (0.716)
	R	−0.007 (0.014)	−0.008 (0.024)	−0.012 (0.02)	0.529 (0.82)	0.626 (0.136)	0.523 (0.915)
Medial parietal	L	−0.004 (0.01)	−0.011 (0.015)	−0.012 (0.007)	0.642 (0.185)	0.743 (0.004)	0.536 (0.888)
	R	0.002 (0.02)	0 (0.024)	−0.003 (0.016)	0.504 (0.988)	0.554 (0.518)	0.536 (0.888)
Occipital lobe	L	−0.005 (0.007)	−0.007 (0.014)	−0.009 (0.01)	0.502 (0.988)	0.625 (0.136)	0.618 (0.595)
	R	−0.005 (0.007)	−0.008 (0.011)	−0.007 (0.01)	0.602 (0.33)	0.596 (0.265)	0.523 (0.915)
Caudate	L	−0.007 (0.015)	−0.025 (0.019)	−0.014 (0.009)	0.781 (0.009)	0.73 (0.006)	0.695 (0.307)
	R	−0.004 (0.013)	−0.01 (0.022)	−0.011 (0.012)	0.672 (0.11)	0.707 (0.013)	0.573 (0.81)
Putamen	L	−0.001 (0.016)	−0.026 (0.015)	−0.014 (0.015)	0.912 (<0.001)	0.739 (0.004)	0.705 (0.302)
	R	−0.002 (0.015)	−0.022 (0.017)	−0.014 (0.019)	0.854 (0.001)	0.712 (0.011)	0.618 (0.595)
Thalamus	L	−0.011 (0.016)	−0.029 (0.024)	−0.026 (0.012)	0.706 (0.059)	0.784 (0.001)	0.532 (0.888)
	R	−0.01 (0.015)	−0.024 (0.021)	−0.016 (0.02)	0.696 (0.071)	0.617 (0.165)	0.591 (0.701)

Results are shown as median (IQR). Brain atrophy is represented as negative values. All *P*-values are corrected using the false discovery rate.
AUROC = area under the receiver operating characteristic curve; Hem = hemisphere; L = left; R = right.

thalamus. The voxel-level maps demonstrate overlap with agPPA in the posterior frontal lobes, basal ganglia and brainstem, but show less involvement of the temporoparietal cortices in PPAOS compared to controls (Fig. 1). On direct comparison between agPPA and PPAOS, the agPPA group showed greater rates of atrophy in left Broca's area, middle frontal gyrus, superior frontal gyrus and medial temporal lobe, compared to PPAOS at the region of interest level (Table 2). Left Broca's area and left middle frontal gyrus were also found to have increased atrophy rates in agPPA compared to PPAOS in the voxel-level maps, although only at an uncorrected threshold of $P < 0.001$ (Fig. 1). There was also evidence of greater atrophy in the anterior cingulate gyrus, left inferior parietal lobe, and temporal lobe in agPPA compared to PPAOS (Fig. 1). No regions showed greater rates in PPAOS compared to agPPA.

Diffusion tensor imaging

A summary of the region of interest level DTI results for all four metrics is shown in Table 3. Detailed region of interest level results for each metric are shown in Supplementary Tables 1–4. Greater rates of change in agPPA compared to controls were identified across most of the DTI metrics in bilateral inferior and middle frontal white matter, bilateral

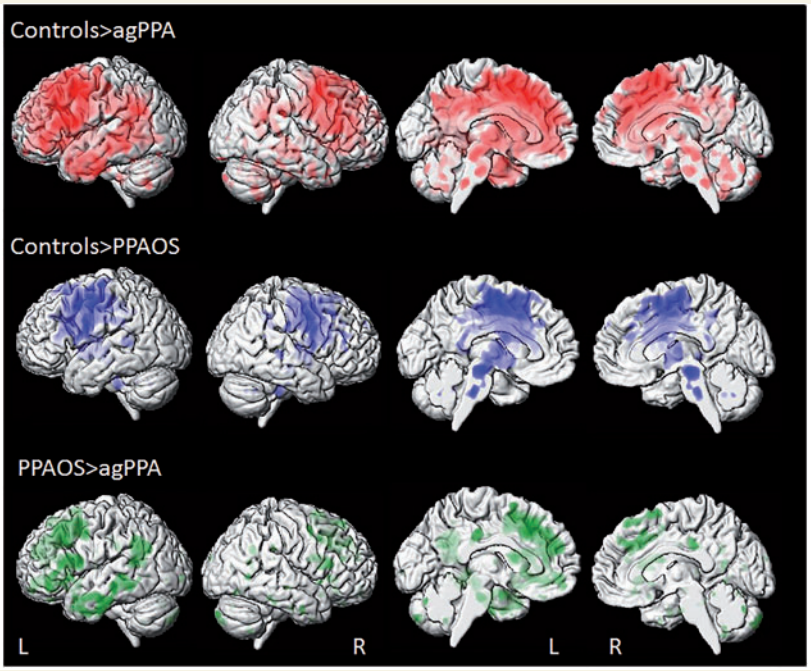

Figure 1 3D surface renderings of the brain showing annualized rates of atrophy in agPPA and PPAOS. Lateral views are shown in the first two columns, and medial views in columns three and four. Results comparing agPPA and PPAOS to controls are shown after correction for multiple comparisons using the false discovery rate correction at $P < 0.01$, and results comparing agPPA to PPAOS are shown uncorrected at $P < 0.001$. *Top row* shows voxels in which rates of brain atrophy are greater in agPPA compared to controls. *Middle row* shows voxels in which rates of brain atrophy are greater in PPAOS compared to controls. *Bottom row* shows voxels in which rates brain atrophy are greater in agPPA compared to PPAOS. L = left; R = right.

superior longitudinal fasciculus, and right superior frontal white matter, inferior fronto-occipital fasciculus, precentral white matter and left external capsule. Some significant findings were also identified in the left fronto-occipital fasciculus (radial diffusivity), right cingulum (fractional anisotropy and radial diffusivity), and left corticospinal tract (fractional anisotropy and axial diffusivity). Greater rates of change in left precentral, superior frontal and parietal white matter, right uncinate fasciculus, and right posterior limb of the internal capsule were observed only with axial diffusivity. The voxel-based analysis also showed greater rates of change in all DTI metrics bilaterally throughout the white matter of the frontal lobes (Fig. 2). Changes were also observed in temporal and parietal white matter, particularly in the left hemisphere, bilateral posterior corpus callosum, cingulum, and midbrain, with the most widespread findings observed in mean, radial and axial diffusivity.

The PPAOS group showed more focal DTI abnormalities, mainly restricted to bilateral superior frontal white matter, superior longitudinal fasciculus, precentral white matter and left external capsule, compared to controls, with more widespread changes observed with axial diffusivity. The voxel-based analyses showed rates of change in premotor regions of both hemispheres, as well as anterior and posterior limbs of the internal capsule, and some involvement of temporoparietal cortex, in PPAOS compared to controls, with the most widespread findings observed in mean, radial and axial diffusivity (Fig. 2). On direct comparison between agPPA and PPAOS at the region of interest level analysis, agPPA showed greater rates of increase in radial diffusivity in left middle frontal white matter and right interior frontal white matter compared to PPAOS (Table 3 and Supplementary Table 3). No differences were observed in fractional anisotropy, mean diffusivity or axial diffusivity. In the voxel-based results, greater rates of increase in radial and axial diffusivity were observed in inferior, middle and superior frontal white matter and posterior limb of the internal capsule in agPPA compared to PPAOS (Fig. 2), with differences greatest in the left hemisphere. Greater rates of increase in mean diffusivity were observed in the left inferior frontal white matter in agPPA compared to PPAOS. No differences were observed in fractional anisotropy. No regions showed greater rates in PPAOS compared to agPPA.

FDG-PET

At the region of interest level (Table 4), agPPA showed a greater decrease in FDG metabolism over time compared to controls across all frontal regions, as well as anterior and middle cingulate, insula, supplementary motor area, rolandic operculum, precentral cortex, lateral temporal lobe, lateral and medial parietal lobe, caudate, putamen and

Table 3 Summary of statistically significant results for each DTI metric

Region of interest	Hem	agPPA ~ Control				PPAOS ~ Control				agPPA ~ PPAOS			
		FA	MD	RD	AxD	FA	MD	RD	AxD	FA	MD	RD	AxD
Inferior frontal white matter	L	0.90	0.85	0.75	0.76								
	R	0.88	0.90	0.93	0.89				0.73			0.86	
Inferior fronto-occipital fasciculus	L			0.79									
	R	0.89		0.75	0.81				0.71				
Middle frontal white matter	L	0.86	0.84	0.86	0.86				0.74			0.88	
	R	0.93	0.78	0.83					0.84				
Middle fronto-orbital white matter	L												
	R												
Superior frontal white matter	L				0.80			0.74	0.75				
	R	0.77	0.86	0.87	0.82			0.78	0.77				
Superior fronto-occipital fasciculus	L			0.78									
	R												
Superior longitudinal fasciculus	L	0.80			0.79	0.83	0.80		0.81				
	R	0.86		0.79	0.79	0.78	0.74		0.76				
Lateral fronto-orbital white matter	L												
	R												
Cingulum	L												
	R	0.80		0.76									
Body of corpus callosum													
Genu of corpus callosum													
Splenium of corpus callosum													
Precentral	L				0.77	0.90	0.84		0.89				
	R	0.78	0.83	0.77	0.80	0.80	0.80		0.88				
Postcentral	L												
	R							0.77					
Corticospinal tract	L	0.80			0.88								
	R				0.84								
Temporal	L												
	R												
Parietal	L				0.78				0.76				
	R				0.82	0.75			0.77				
Occipital	L												
	R												
Uncinate fasciculus	L												
	R				0.77				0.73				
Posterior thalamic radiation	L												
	R												
Superior cerebellar peduncle	L	0.86											
	R												
Anterior limb of internal capsule	L												
	R												
Posterior limb of internal capsule	L						0.74						
	R				0.78		0.73						
External capsule	L	0.79	0.83	0.77			0.76	0.73					
	R				0.77								

AUROC values are provided when a comparison was statistically significant (false discovery rate correction P-value < 0.05). All raw AUROCS and P-values are provided in Supplementary Tables 1–4. AxD = axial diffusivity; FA = fractional anisotropy; Hem = hemisphere; L = left; MD = mean diffusivity; R = right; RD = radial diffusivity.

thalamus. Rates of change were greater in the left hemisphere, but showed faster rates compared to controls in both hemispheres across frontal regions. The voxel-based analysis similarly showed greater rates of change in metabolism bilaterally throughout the frontal lobes, with greater rates in the left hemisphere, as well as in the left temporoparietal cortex, in agPPA compared to controls (Fig. 3).

In the region of interest level analysis, the PPAOS subjects showed a greater decrease in FDG metabolism over time compared to controls only in bilateral supplementary motor area, precentral cortex and left thalamus (Table 4). The voxel-level analysis similarly showed rates of change restricted to the posterior frontal lobes, with some incidental findings around the edge of the ventricles (Fig. 3). On direct comparison between agPPA and PPAOS, the agPPA group showed greater rates of change in left Broca's area, middle frontal gyrus, superior frontal gyrus, superior medial frontal gyrus, orbitofrontal cortex, anterior and

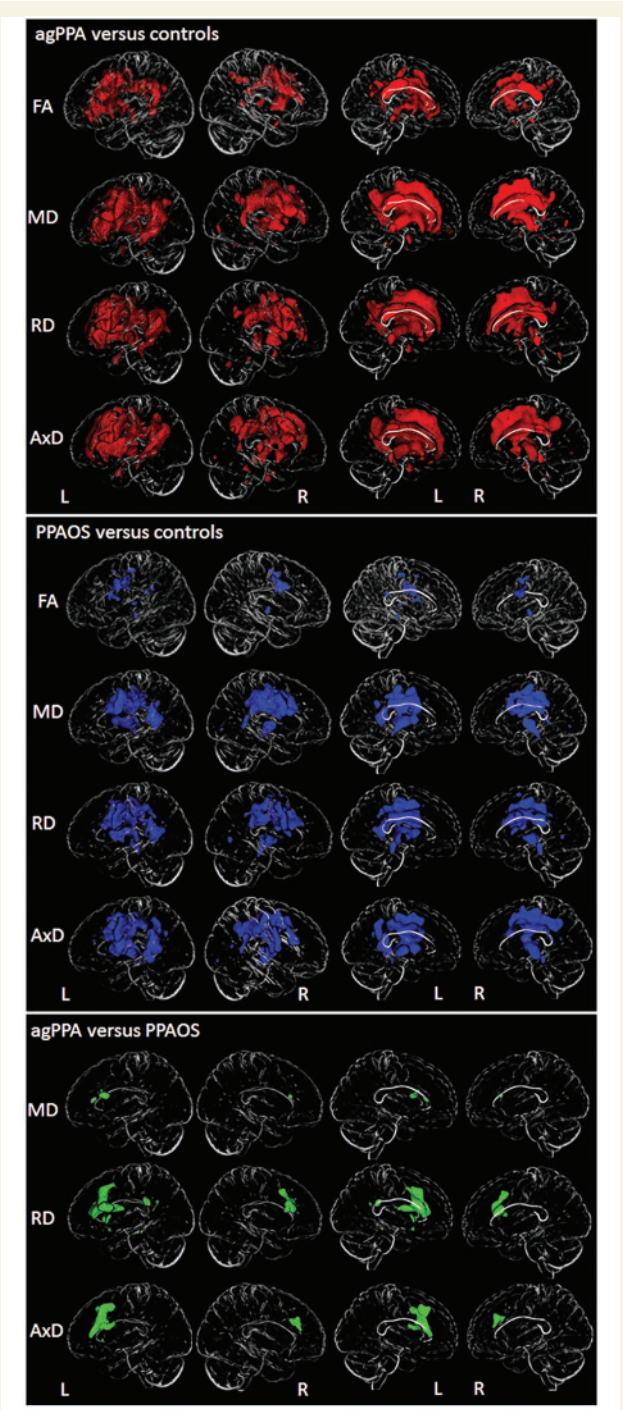

Figure 2 3D brain skeletons showing annualized rates of decline in white matter fractional anisotropy and annualized rates of increase in mean diffusivity, radial diffusivity and axial diffusivity in agPPA and PPAOS. Lateral views are shown in the first two columns, and medial views in columns three and four. All results are shown after correction for multiple comparisons using the false discovery rate correction at $P < 0.01$. Results in red show voxels in which rates of change are greater in agPPA compared to controls. Results in blue show voxels in which rates of change are greater in PPAOS compared to controls. Results in green show voxels in which rates of change are greater in agPPA compared to PPAOS. AxD = axial diffusivity; FA = fractional anisotropy; L = left; MD = mean diffusivity; R = right; RD = radial diffusivity.

middle cingulate, insula, supplementary motor area, and lateral parietal lobe compared to PPAOS (Table 4). Increased rates of change were also observed throughout the lateral and medial frontal lobe and parietal lobe in agPPA compared to PPAOS in the voxel-level analysis, although these results did not survive correction for multiple comparisons and are, hence, shown at an uncorrected threshold of $P < 0.001$ (Fig. 3). We observed the same differences between agPPA and PPAOS using partial-volume corrected data. No regions showed greater rates in PPAOS compared to agPPA.

Clinical correlations

The results of the clinical correlations are shown in Fig. 4. Rate of decline in WAB-AQ was associated with faster rates of atrophy and faster decline in metabolism bilaterally throughout the prefrontal cortices and in the middle temporal and supramarginal gyri across the entire cohort (uncorrected $P < 0.001$ and FDR $P < 0.01$). In the DTI analyses, faster rate of decline in WAB-AQ was associated with greater rates of change in all DTI metrics bilaterally in frontal lobe white matter, particularly in inferior frontal gyri, and with left temporal white matter in mean, radial and axial diffusivity across the entire cohort (uncorrected $P < 0.001$). We observed topographically similar results with findings in the frontal and temporal lobes when the correlations were restricted to only agPPA subjects, although at a more lenient statistical threshold given the smaller number of subjects and reduced power (Supplementary Fig. 1).

Faster rate of increase in MDS-UPDRS part III was associated with faster rates of atrophy and faster decline in metabolism predominantly in left superior motor cortex across the entire cohort (uncorrected $P < 0.001$). In the DTI analyses, faster rate of increase in MDS-UPDRS II was associated with greater rates of fractional anisotropy decline and mean, radial and axial diffusivity increase in bilateral motor cortex, cerebral peduncle, and brainstem white matter across the entire cohort (uncorrected $P < 0.001$), with right internal capsule also identified with fractional anisotropy (FDR $P < 0.01$).

Faster rate of decline in the WAB-apraxia score was associated with greater rates of atrophy bilaterally in motor cortex, and faster decline in metabolism in supplementary motor area, across the entire cohort (uncorrected $P < 0.001$). In the DTI analyses, faster rate of decline in WAB-apraxia was associated with greater rates of fractional anisotropy decline in motor cortex white matter, as well as in middle cingulum, internal capsule, cerebral peduncle and occipital white matter across the entire cohort (uncorrected $P < 0.001$, motor white matter FDR $P < 0.01$). Faster rate of decline in WAB-apraxia was also associated with greater rates of mean, radial and axial diffusivity increase in motor cortex and brainstem white matter across the entire cohort (uncorrected $P < 0.001$ and FDR $P < 0.01$).

Table 4 Annualized rates of change in FDG metabolism across regions of interest

Region of interest	Hem	Control	agPPA	PPAOS	agPPA ~ Control	PPAOS ~ Control	agPPA ~ PPAOS
					AUROC (*P*)	AUROC (*P*)	AUROC (*P*)
Broca's area	L	−0.006 (0.041)	−0.081 (0.028)	−0.02 (0.029)	0.934 (<0.001)	0.631 (0.222)	0.945 (<0.001)
	R	−0.004 (0.043)	−0.056 (0.041)	−0.019 (0.036)	0.812 (0.003)	0.59 (0.375)	0.745 (0.089)
Middle frontal	L	−0.011 (0.049)	−0.094 (0.041)	−0.026 (0.035)	0.908 (<0.001)	0.615 (0.289)	0.895 (0.002)
	R	−0.01 (0.051)	−0.064 (0.056)	−0.023 (0.037)	0.752 (0.015)	0.554 (0.509)	0.705 (0.162)
Superior frontal	L	−0.009 (0.041)	−0.069 (0.044)	−0.018 (0.032)	0.853 (0.001)	0.584 (0.382)	0.836 (0.009)
	R	−0.005 (0.044)	−0.049 (0.039)	−0.022 (0.033)	0.757 (0.014)	0.602 (0.328)	0.695 (0.185)
Superior medial frontal	L	−0.004 (0.039)	−0.07 (0.038)	−0.017 (0.025)	0.9 (<0.001)	0.606 (0.327)	0.868 (0.005)
	R	−0.007 (0.036)	−0.05 (0.034)	−0.016 (0.03)	0.806 (0.004)	0.565 (0.509)	0.768 (0.053)
Orbitofrontal cortex	L	−0.002 (0.042)	−0.062 (0.05)	−0.011 (0.032)	0.815 (0.003)	0.554 (0.509)	0.777 (0.045)
	R	−0.002 (0.041)	−0.03 (0.048)	−0.013 (0.031)	0.651 (0.154)	0.565 (0.509)	0.605 (0.471)
Anterior cingulate	L	0 (0.039)	−0.05 (0.038)	−0.003 (0.023)	0.833 (0.002)	0.555 (0.509)	0.836 (0.009)
	R	−0.003 (0.041)	−0.038 (0.055)	−0.008 (0.032)	0.679 (0.085)	0.591 (0.375)	0.636 (0.367)
Middle cingulate	L	−0.002 (0.042)	−0.058 (0.024)	−0.029 (0.025)	0.89 (<0.001)	0.699 (0.054)	0.791 (0.034)
	R	−0.007 (0.039)	−0.044 (0.048)	−0.026 (0.028)	0.713 (0.043)	0.656 (0.158)	0.6 (0.484)
Insula	L	−0.006 (0.033)	−0.058 (0.027)	−0.013 (0.029)	0.922 (<0.001)	0.593 (0.375)	0.895 (0.002)
	R	−0.006 (0.031)	−0.034 (0.026)	−0.017 (0.027)	0.768 (0.01)	0.594 (0.375)	0.686 (0.21)
Supplementary motor area	L	−0.006 (0.042)	−0.071 (0.025)	−0.04 (0.023)	0.912 (<0.001)	0.788 (0.005)	0.855 (0.006)
	R	−0.008 (0.04)	−0.064 (0.041)	−0.038 (0.025)	0.855 (0.001)	0.768 (0.007)	0.682 (0.218)
Rolandic operculum	L	0 (0.041)	−0.031 (0.047)	−0.026 (0.033)	0.71 (0.045)	0.687 (0.075)	0.545 (0.851)
	R	−0.001 (0.038)	−0.027 (0.051)	−0.02 (0.033)	0.628 (0.225)	0.64 (0.188)	0.518 (0.955)
Precentral	L	−0.007 (0.04)	−0.053 (0.044)	−0.032 (0.024)	0.802 (0.004)	0.742 (0.017)	0.673 (0.235)
	R	−0.004 (0.042)	−0.049 (0.047)	−0.032 (0.029)	0.776 (0.008)	0.708 (0.046)	0.609 (0.471)
Postcentral	L	−0.007 (0.038)	−0.037 (0.045)	−0.017 (0.031)	0.699 (0.055)	0.586 (0.375)	0.627 (0.391)
	R	−0.004 (0.041)	−0.033 (0.049)	−0.021 (0.03)	0.644 (0.174)	0.66 (0.154)	0.527 (0.91)
Paracentral lobule	L	−0.003 (0.04)	−0.017 (0.035)	−0.006 (0.032)	0.581 (0.481)	0.524 (0.75)	0.605 (0.471)
	R	−0.004 (0.034)	−0.008 (0.044)	−0.013 (0.036)	0.512 (0.908)	0.527 (0.743)	0.541 (0.851)
Lateral temporal	L	−0.002 (0.031)	−0.026 (0.026)	−0.01 (0.021)	0.745 (0.018)	0.586 (0.375)	0.727 (0.111)
	R	0 (0.028)	−0.005 (0.03)	−0.012 (0.022)	0.519 (0.868)	0.623 (0.267)	0.627 (0.391)
Medial temporal	L	−0.001 (0.021)	−0.015 (0.017)	−0.004 (0.017)	0.702 (0.053)	0.558 (0.509)	0.668 (0.244)
	R	−0.003 (0.022)	−0.006 (0.021)	−0.006 (0.019)	0.532 (0.797)	0.541 (0.615)	0.505 (1)
Lateral parietal	L	−0.006 (0.039)	−0.055 (0.029)	−0.02 (0.027)	0.872 (<0.001)	0.603 (0.328)	0.814 (0.018)
	R	−0.005 (0.039)	−0.032 (0.05)	−0.024 (0.029)	0.632 (0.213)	0.644 (0.188)	0.514 (0.965)
Medial parietal	L	−0.003 (0.046)	−0.056 (0.042)	−0.027 (0.03)	0.795 (0.005)	0.65 (0.172)	0.723 (0.115)
	R	−0.008 (0.04)	−0.018 (0.058)	−0.027 (0.034)	0.554 (0.646)	0.61 (0.317)	0.541 (0.851)
Occipital lobe	L	−0.012 (0.049)	−0.017 (0.05)	−0.016 (0.039)	0.521 (0.868)	0.56 (0.509)	0.527 (0.91)
	R	−0.012 (0.048)	−0.006 (0.057)	−0.017 (0.04)	0.553 (0.646)	0.559 (0.509)	0.609 (0.471)
Caudate	L	−0.005 (0.039)	−0.045 (0.029)	−0.015 (0.045)	0.827 (0.002)	0.62 (0.269)	0.727 (0.111)
	R	−0.007 (0.034)	−0.026 (0.029)	−0.011 (0.046)	0.692 (0.064)	0.554 (0.509)	0.641 (0.356)
Putamen	L	0.003 (0.045)	−0.037 (0.026)	−0.016 (0.046)	0.77 (0.01)	0.64 (0.188)	0.673 (0.235)
	R	−0.004 (0.046)	−0.018 (0.054)	−0.012 (0.056)	0.573 (0.52)	0.556 (0.509)	0.5 (1)
Thalamus	L	−0.004 (0.042)	−0.064 (0.024)	−0.037 (0.044)	0.897 (<0.001)	0.727 (0.026)	0.732 (0.111)
	R	−0.009 (0.041)	−0.052 (0.052)	−0.031 (0.047)	0.782 (0.007)	0.68 (0.085)	0.641 (0.356)

Results are shown as median (IQR). Reduced metabolism is represented as negative values. All *P*-values are corrected using the false discovery rate.
Hem = hemisphere; L = left; R = right.

Rate of increase in the ASRS was not associated with any coherent pattern of change in the neuroimaging metrics across the entire cohort.

Discussion

This neuroimaging study characterizes the progression of structural and molecular changes in the brain over time in agPPA and demonstrates progression of grey matter atrophy, white matter degeneration and FDG-PET hypometabolism throughout the language network, as well as to regions outside the language network. These patterns differed from the more focal patterns of progression in PPAOS, which predominantly involved premotor and motor regions. These findings highlight the widespread nature of neurodegeneration in agPPA and support the clinical distinction of agPPA from PPAOS.

When comparing agPPA to controls, both grey matter atrophy and decline in FDG-PET metabolism was found throughout the language network, including inferior and middle frontal gyri and medial and lateral temporal lobe (Dronkers, 2011; Whitwell *et al.*, 2015). We also observed degeneration in white matter tracts that connect regions in the language network, such as the superior longitudinal fasciculus (Dronkers, 2011; Friederici and Gierhan, 2013).

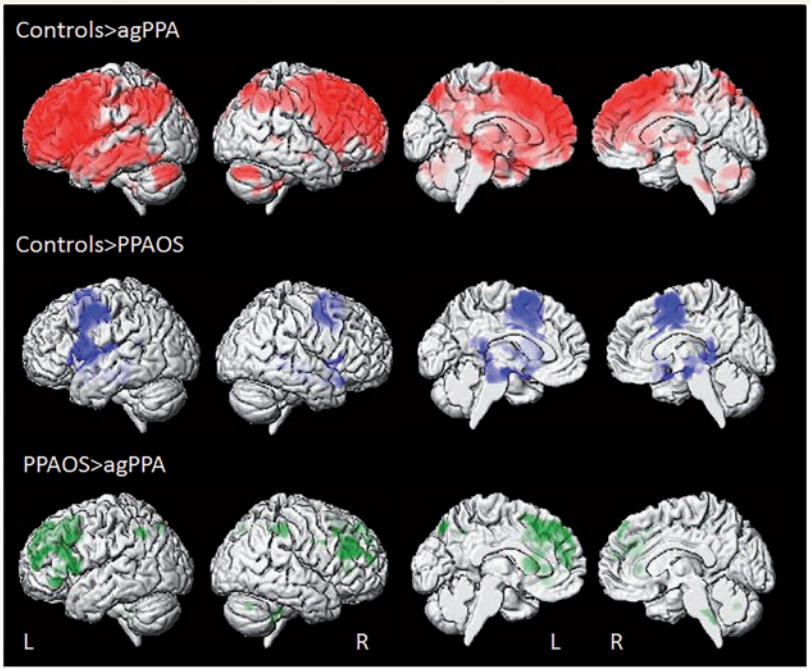

Figure 3 3D surface renderings of the brain showing annualized rates of decline in FDG-PET metabolism in agPPA and PPAOS. Lateral views are shown in the first two columns, and medial views in columns three and four. Results comparing agPPA and PPAOS to controls are shown after correction for multiple comparisons using the false discovery rate correction at $P < 0.01$, and results comparing agPPA to PPAOS are shown uncorrected at $P < 0.001$. *Top row* shows voxels in which rates of decline in metabolism are greater in agPPA compared to controls. *Middle row* shows voxels in which rates of decline in metabolism are greater in PPAOS compared to controls. *Bottom row* shows voxels in which rates of decline in metabolism are greater in agPPA compared to PPAOS. L = left; R = right.

These findings support the conclusion that agPPA spreads via regions that are located in the language connectivity networks (Mandelli *et al.*, 2016). Left-sided asymmetry is typical for agPPA in cross-sectional studies (Gorno-Tempini *et al.*, 2004*a*; Josephs *et al.*, 2006; Mesulam *et al.*, 2008; Botha *et al.*, 2015). Although patterns were largely bilateral in the frontal lobes, this asymmetry remained. These findings are consistent with patterns of frontal and temporal cortical thinning observed over time in agPPA by one group (Rogalski *et al.*, 2011, 2014), although another group found that longitudinal grey matter atrophy was more restricted to the frontal lobe with little temporal lobe involvement (Mandelli *et al.*, 2016). Interestingly, in our cohort, atrophy and decline in metabolism extended beyond the left frontal and temporal lobes into the parietal lobes, motor cortex, basal ganglia, and brainstem. Atrophy in these areas is characteristic of corticobasal degeneration (CBD) (Grossman *et al.*, 2004; Boxer *et al.*, 2006; Josephs *et al.*, 2008*a*) and progressive supranuclear palsy (PSP) (Oba *et al.*, 2005; Boxer *et al.*, 2006; Whitwell *et al.*, 2013*b*), fitting with the fact that individuals with agPPA can develop additional motor symptoms of these neurodegenerative syndromes (Gorno-Tempini *et al.*, 2004*b*; Kertesz *et al.*, 2005; Josephs *et al.*, 2006; Graff-Radford *et al.*, 2012). In fact, our correlation analyses confirmed a link between degeneration of some of these regions and progression of parkinsonism and limb apraxia in our cohort, as discussed in more detail below.

Progression of white matter degeneration was fairly limited to the frontal lobe but was relatively bilateral in its distribution in agPPA. The inferior and middle frontal regions were consistently affected across all four DTI metrics, and have been reported to show abnormal diffusivity in cross-sectional studies (Whitwell *et al.*, 2010; Galantucci *et al.*, 2011; Josephs *et al.*, 2013; Mahoney *et al.*, 2013). Furthermore, the DTI analysis revealed right-sided change in a number of white matter tracts that was relatively consistent across DTI metrics, including inferior fronto-occipital fasciculus, superior frontal white matter, cingulum and precentral white matter. Because the aforementioned cross-sectional studies stressed the left asymmetry in the frontal regions, evidence of increased right hemisphere change over time gives an idea of how agPPA progresses and spreads within the brain, with white matter tract degeneration spreading to the right hemisphere. One previous longitudinal DTI study that demonstrated changes over time in frontal white matter tracts in agPPA also observed greater rates in the right hemisphere (Lam *et al.*, 2014). Our findings also highlight how white matter degeneration is spreading into posterior tracts in the brain, with involvement of precentral white matter and some evidence for involvement of corticospinal tracts and parietal white matter.

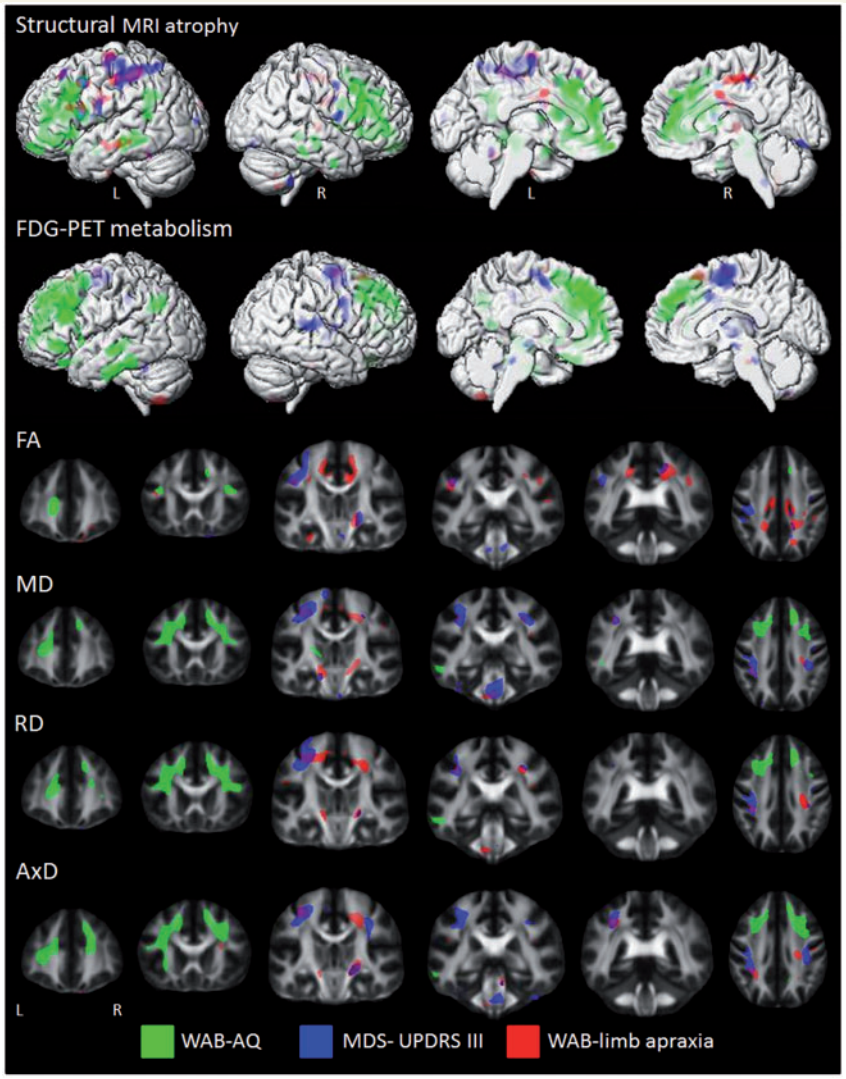

Figure 4 Correlations between rate of change in neuroimaging and clinical measures. Structural MRI results represent regions where faster rates of atrophy correlate with faster worsening of the clinical measures. FDG-PET results represent regions where faster decline in metabolism correlate with faster worsening of the clinical measures. Fractional anisotropy (FA) results represent regions where faster rates of fractional anisotropy decline correlate with faster worsening of the clinical measures. Mean diffusivity (MD), radial diffusivity (RD) and axial diffusivity (AxD) results represent regions where faster rates of increase correlate with faster worsening of the clinical measures. Structural MRI results are shown on three-dimensional surface renderings, while DTI results are shown on a group fractional anisotropy template. Results were generated using the whole cohort and shown uncorrected at $P < 0.001$. AQ = aphasia quotient; L = left; MDS-UPDRS = Movement Disorder Society sponsored revision of the Unified Parkinson's Disease rating scale; R = right; WAB = Western Aphasia Battery.

This mirrors the spread of grey matter atrophy and FDG-PET metabolism. Increased rates of fractional anisotropy decline were also found in the left superior cerebellar peduncle. Again, this could be associated with the development of clinical features of PSP (Tsuboi *et al.*, 2003; Paviour *et al.*, 2005; Whitwell *et al.*, 2011, 2014). The lack of significant mean, radial or axial diffusivity findings in this region may suggest that a directional diffusion measure is more sensitive to deficits in this tract.

The regional DTI findings in agPPA were largely concordant across the different DTI metrics. Interestingly, fractional anisotropy tended to show the least widespread patterns of change in the voxel-maps, although showed equivalent or higher AUROCs than the other metrics in a number of the implicated tracts. In addition, changes in temporal and parietal white matter tracts and the posterior limb of the internal capsule were only significant for axial diffusivity, which has been suggested to be a measure of axonal degeneration (Song *et al.*, 2003). The interpretation of these differences is unclear, although it may suggest that axial diffusivity is the most sensitive DTI metric to capture widespread longitudinal changes in agPPA. Similarly, we observed more widespread changes in axial diffusivity compared to the other DTI metrics in PPAOS. However, in

contrast, a previous study found that fractional anisotropy and radial diffusivity revealed the most prominent changes over time in agPPA, with very few longitudinal changes observed in axial diffusivity (Lam *et al.*, 2014). The lack of consistency across studies may be due to methodological differences, since the previous study used tract-based spatial statistics to independently transform each time-point for comparison, rather than our TBM approach of directly analysing within-subject non-linear deformations across time points. This inconsistency suggests caution should be applied in drawing conclusions about the relevance of these DTI metrics to specific underlying disease processes.

Regions were identified that showed greater rates of change in agPPA compared to PPAOS after correction for multiple comparisons in all three imaging modalities. The areas with the most striking difference in grey matter atrophy rates were Broca's area, middle frontal gyrus, superior frontal gyrus and insula, with all regions showing greater rates of atrophy in agPPA. The FDG-PET analysis also identified differences in these regions, as well as other frontal, cingulate, premotor and parietal regions. Given the role of Broca's area in syntactic comprehension and production (Embick *et al.*, 2000; Friederici *et al.*, 2003; Rogalsky and Hickok, 2011), and its relationship to agrammatism in PPA (Whitwell *et al.*, 2013*a*; Flinker *et al.*, 2015), it makes sense that this region would show greater degeneration over time in agPPA, since these patients also showed faster rates of decline in the WAB-AQ, compared to PPAOS. Agrammatism can eventually develop in people with PPAOS (Josephs *et al.*, 2014); this was evidenced by progression on the WAB-AQ and Token Test over time, although notably the progression was less severe than that observed in agPPA. Differences observed between the two syndromes in other frontal, temporal and parietal regions suggest that spreading of degeneration throughout the language network is a feature more strongly associated with agPPA than PPAOS. The agPPA group also showed greater rates of change in the DTI metrics, although differences were limited to the inferior and middle frontal white matter and differences were greatest for radial diffusivity and axial diffusivity. Therefore, it appears as though agPPA is associated with greater degeneration over time in both grey and white matter regions of the language network. The more widespread differences and high AUROCs observed in the FDG-PET analyses, however, suggest that this modality may be the best one to use to differentiate agPPA and PPAOS.

It is also clear when comparing agPPA and PPAOS against controls that the patterns of progression are quite different between these two syndromes, with agPPA showing progression throughout the language network and more focal patterns of progression observed in PPAOS. However, we also observed overlap between the two syndromes, with progression in Broca's area, cingulate gyrus, supplementary motor areas, precentral cortex, and the brainstem in both syndromes when compared to controls. This overlap is consistent with the overlapping clinical features of these syndromes; six of the subjects in the agPPA cohort presented with ancillary AOS at baseline examination, and eight of the PPAOS subjects, who were all diagnosed with isolated PPAOS at baseline examination, had developed some agrammatism by the follow-up examination, although the AOS remained their predominant problem. Similarly, there was white matter tract degeneration overlap between the two groups in the superior longitudinal fasciculus, showing that degeneration of this tract is a feature of both syndromes. Nevertheless, despite some degree of overlap between agPPA and PPAOS from both a clinical and imaging standpoint, they clearly show different patterns of progression, ultimately supporting the syndromic distinction.

Our correlation analyses provided unique insight into the neurobiological underpinnings of the progression of clinical symptoms we observed in our agPPA and PPAOS cohorts. We observed a clear dissociation in brain regions associated with progression of aphasia versus progression of motor symptoms (i.e. parkinsonism and limb apraxia) with the former associated with bilateral degeneration of frontal, temporal and parietal regions within the language network, and the later associated with degeneration of motor cortex and brainstem. This demonstrates that disease progression is not isolated to just the language network (Mandelli *et al.*, 2016), but also spreads to involve networks related to motor function, which are responsible for the development of clinical features of CBD and PSP that are often observed in these subjects. Progression of parkinsonism was associated with progressive deterioration of the white matter underlying motor cortex, as well as white matter tracts in the internal capsule, cerebral peduncle and brainstem, suggesting involvement of the corticospinal tracts. These white matter regions were also associated with progression of limb apraxia, although we observed less involvement of the brainstem corticospinal tracts and additional patterns of white matter damage underling the cortex that may suggest a breakdown of cortico-cortical connections, as others have postulated (Pramstaller and Marsden, 1996; Leiguarda, 2001). This is the first study to assess such longitudinal clinical imaging correlations in these patients. One previous cross-sectional study found that limb apraxia correlated with parietal grey matter volume in agPPA (Rohrer *et al.*, 2010), although the findings may have been influenced by the inclusion of patients with corticobasal syndrome (Borroni *et al.*, 2008). Our previous cross-sectional studies have shown that severity of AOS correlates with atrophy in supplementary motor area and premotor cortex (Josephs *et al.*, 2006, 2012, 2014); although in this study we did not identify any coherent neuroanatomical correlates with progression of AOS. The lack of longitudinal correlations could be due to variability across subjects in the specific characteristics of AOS (Josephs *et al.*, 2013) or because the measures are reliant on speakers being able to produce enough speech to demonstrate the features rated; speech was extremely limited in some subjects with AOS.

The present study has several strengths; all subjects were evaluated by an experienced speech-language pathologist and underwent a detailed battery of speech and language tests. Our agPPA cohort was relatively pure, with all subjects having agrammatism that was equal to or greater than the AOS, if any AOS was present. Likewise, the PPAOS controls all had isolated AOS at baseline with no agrammatism, and if agrammatism developed, it remained less severe than the AOS. An additional strength was that we analysed annualized rates of change across the entire brain, using both region of interest and voxel-based analyses, and we used DTI to assess white matter tract integrity. The biggest limitation of the study was the small number of agPPA subjects, although our cohort of 11 is actually larger than many other studies investigating imaging characteristics of this syndrome, which have ranged from three to nine agPPA subjects (Galantucci *et al.*, 2011; Rogalski *et al.*, 2011, 2014; Brambati *et al.*, 2015). The relatively small number of agPPA subjects limited our power to detect clinical-imaging correlations within this group.

In summary, we have characterized the longitudinal patterns of structural and molecular degeneration in agPPA, which increases knowledge of the underlying biological progression of this syndrome and the relationship between progression of brain degeneration and progression of clinical symptoms. Our findings also support the notion that subjects with agPPA and PPAOS should not compose one but two unique diagnostic categories, even though the syndromes share some clinical and imaging features.

Acknowledgements

We would like to acknowledge Stephen D. Weigand, Mayo Clinic, for providing statistical advice and Drs Ronald Petersen, David Knopman, Bradley Boeve, Jon Graff-Radford, and David Jones for performing clinical evaluations on the healthy controls.

Funding

This study was funded by National Institutes of Health grants R01-DC12519, R01-DC010367, R01-AG11378, R21-NS94684 and U01-AG006786.

Supplementary material

Supplementary material is available at *Brain* online.

References

Acion L, Peterson JJ, Temple S, Arndt S. Probabilistic index: an intuitive non-parametric approach to measuring the size of treatment effects. Stat Med 2006; 25: 591–602.

Amici S, Brambati SM, Wilkins DP, Ogar J, Dronkers NL, Miller BL, et al. Anatomical correlates of sentence comprehension and verbal working memory in neurodegenerative disease. J Neurosci 2007; 27: 6282–90.

Ashburner J, Friston KJ. Unified segmentation. Neuroimage 2005; 26: 839–51.

Avants BB, Epstein CL, Grossman M, Gee JC. Symmetric diffeomorphic image registration with cross-correlation: evaluating automated labeling of elderly and neurodegenerative brain. Med Image Anal 2008; 12: 26–41.

Borroni B, Garibotto V, Agosti C, Brambati SM, Bellelli G, Gasparotti R, et al. White matter changes in corticobasal degeneration syndrome and correlation with limb apraxia. Arch Neurol 2008; 65: 796–801.

Botha H, Duffy JR, Whitwell JL, Strand EA, Machulda MM, Schwarz CG, et al. Classification and clinicoradiologic features of primary progressive aphasia (PPA) and apraxia of speech. Cortex 2015; 69: 220–36.

Boxer AL, Geschwind MD, Belfor N, Gorno-Tempini ML, Schauer GF, Miller BL, et al. Patterns of brain atrophy that differentiate corticobasal degeneration syndrome from progressive supranuclear palsy. Arch Neurol 2006; 63: 81–6.

Brambati SM, Amici S, Racine CA, Neuhaus J, Miller Z, Ogar J, et al. Longitudinal gray matter contraction in three variants of primary progressive aphasia: a tenser-based morphometry study. Neuroimage Clin 2015; 8: 345–55.

Cash DM, Frost C, Iheme LO, Ünay D, Kandemir M, Fripp J, et al. Assessing atrophy measurement techniques in dementia: results from the MIRIAD atrophy challenge. Neuroimage 2015; 123: 149–64.

De Renzi A, Vignolo LA. Token test: a sensitive test to detect receptive disturbances in aphasics. Brain 1962; 85: 665–78.

Dronkers NF. The neural architecture of the language comprehension network: converging evidence from lesion and connectivity analyses. Front Syst Neurosci 2011; 5: 1.

Dubois B, Slachevsky A, Litvan I, Pillon B. The FAB: a Frontal Assessment Battery at bedside. Neurology 2000; 55: 1621–6.

Duffy J. Motor speech disorders: substrates. differential diagnosis, and management. St Louis, MO: Elsevier Mosby; 2005.

Duffy JR, Strand EA, Josephs KA. Motor speech disorders associated with primary progressive aphasia. Aphasiology 2014; 28: 1004–17.

Embick D, Marantz A, Miyashita Y, O'Neil W, Sakai KL. A syntactic specialization for Broca's area. Proc Natl Acad Sci USA 2000; 97: 6150–4.

Flinker A, Korzeniewska A, Shestyuk AY, Franaszczuk PJ, Dronkers NF, Knight RT, et al. Redefining the role of Broca's area in speech. Proc Natl Acad Sci USA 2015; 112: 2871–5.

Friederici AD, Gierhan SM. The language network. Curr Opin Neurobiol 2013; 23: 250–4.

Friederici AD, Rueschemeyer SA, Hahne A, Fiebach CJ. The role of left inferior frontal and superior temporal cortex in sentence comprehension: localizing syntactic and semantic processes. Cereb Cortex 2003; 13: 170–7.

Galantucci S, Tartaglia MC, Wilson SM, Henry ML, Filippi M, Agosta F, et al. White matter damage in primary progressive aphasias: a diffusion tensor tractography study. Brain 2011; 134 (Pt 10): 3011–29.

Garyfallidis E, Brett M, Amirbekian B, Rokem A, Van Der Walt S, Descoteaux M, et al. Dipy, a library for the analysis of diffusion MRI data. Front Neuroinform 2014; 8: 8.

Goetz CG, Tilley BC, Shaftman SR, Stebbins GT, Fahn S, Martinez-Martin P, et al. Movement Disorder Society-sponsored revision of the Unified Parkinson's Disease Rating Scale (MDS-UPDRS): scale presentation and clinimetric testing results. Mov Disord 2008; 23: 2129–70.

Gorno-Tempini ML, Dronkers NF, Rankin KP, Ogar JM, Phengrasamy L, Rosen HJ, et al. Cognition and anatomy in three variants of primary progressive aphasia. Ann Neurol 2004a; 55: 335–46.

Gorno-Tempini ML, Hillis AE, Weintraub S, Kertesz A, Mendez M, Cappa SF, et al. Classification of primary progressive aphasia and its variants. Neurology 2011; 76: 1006–14.

Gorno-Tempini ML, Murray RC, Rankin KP, Weiner MW, Miller BL. Clinical, cognitive and anatomical evolution from nonfluent progressive aphasia to corticobasal syndrome: a case report. Neurocase 2004b; 10: 426–36.

Graff-Radford J, Duffy JR, Strand EA, Josephs KA. Parkinsonian motor features distinguish the agrammatic from logopenic variant of primary progressive aphasia. Parkinsonism Relat Disord 2012; 18: 890–2.

Grossman M, McMillan C, Moore P, Ding L, Glosser G, Work M, et al. What's in a name: voxel-based morphometric analyses of MRI and naming difficulty in Alzheimer's disease, frontotemporal dementia and corticobasal degeneration. Brain 2004; 127: 628–49.

Hughes CP, Berg L, Danziger WL, Coben LA, Martin RL. A new clinical scale for the staging of dementia. Br J Psychiatry 1982; 140: 566–72.

Jack CR, Lowe VJ, Senjem ML, Weigand SD, Kemp BJ, Shiung MM, et al. 11C PiB and structural MRI provide complementary information in imaging of Alzheimer's disease and amnestic mild cognitive impairment. Brain 2008; 131: 665–80.

Jack CR Jr, Wiste HJ, Knopman DS, Vemuri P, Mielke MM, Weigand SD, et al. Rates of beta-amyloid accumulation are independent of hippocampal neurodegeneration. Neurology 2014; 82: 1605–12.

Josephs KA, Duffy JR, Strand EA, Machulda MM, Senjem ML, Gunter JL, et al. The evolution of primary progressive apraxia of speech. Brain 2014; 137 (Pt 10): 2783–95.

Josephs KA, Duffy JR, Strand EA, Machulda MM, Senjem ML, Lowe VJ, et al. Syndromes dominated by apraxia of speech show distinct characteristics from agrammatic PPA. Neurology 2013; 81: 337–45.

Josephs KA, Duffy JR, Strand EA, Machulda MM, Senjem ML, Master AV, et al. Characterizing a neurodegenerative syndrome: primary progressive apraxia of speech. Brain 2012; 135 (Pt 5): 1522–36.

Josephs KA, Duffy JR, Strand EA, Whitwell JL, Layton KF, Parisi JE, et al. Clinicopathological and imaging correlates of progressive aphasia and apraxia of speech. Brain 2006; 129 (Pt 6): 1385–98.

Josephs KA, Whitwell JL, Dickson DW, Boeve BF, Knopman DS, Petersen RC, et al. Voxel-based morphometry in autopsy proven PSP and CBD. Neurobiol Aging 2008a; 29: 280–9.

Josephs KA, Whitwell JL, Duffy JR, Vanvoorst WA, Strand EA, Hu WT, et al. Progressive aphasia secondary to Alzheimer disease vs FTLD pathology. Neurology 2008b; 70: 25–34.

Jung Y, Duffy JR, Josephs KA. Primary progressive aphasia and apraxia of speech. Semin Neurol 2013; 33: 342–7.

Kaufer DI, Cummings JL, Ketchel P, Smith V, MacMillan A, Shelley T, et al. Validation of the NPI-Q, a brief clinical form of the Neuropsychiatric Inventory. J Neuropsychiatry Clin Neurosci 2000; 12: 233–9.

Kertesz A. Western Aphasia Battery (Revised). San Antonio, Tx: PsychCorp; 2007.

Kertesz A, McMonagle P, Blair M, Davidson W, Munoz DG. The evolution and pathology of frontotemporal dementia. Brain 2005; 128: 1996–2005.

Lam BY, Halliday GM, Irish M, Hodges JR, Piguet O. Longitudinal white matter changes in frontotemporal dementia subtypes. Hum Brain Mapp 2014; 35: 3547–57.

Lansing AE, Ivnik RJ, Cullum CM, Randolph C. An empirically derived short form of the Boston naming test. Arch Clin Neuropsychol 1999; 14: 481–7.

Leiguarda R. Limb apraxia: cortical or subcortical. Neuroimage 2001; 14 (1 Pt 2): S137–41.

Lewis EB, Fox NC. Correction of differential intensity inhomogeneity in longitudinal MR images. Neuroimage 2004; 23: 75–83.

Mahoney CJ, Malone IB, Ridgway GR, Buckley AH, Downey LE, Golden HL, et al. White matter tract signatures of the progressive aphasias. Neurobiol Aging 2013; 34: 1687–99.

Mandelli ML, Vilaplana E, Brown JA, Hubbard HI, Binney RJ, Attygalle S, et al. Healthy brain connectivity predicts atrophy progression in non-fluent variant of primary progressive aphasia. Brain 2016; 139 (Pt 10): 2778–91.

Meltzer CC, Leal JP, Mayberg HS, Wagner HN Jr, Frost JJ. Correction of PET data for partial volume effects in human cerebral cortex by MR imaging. J Comput Assist Tomogr 1990; 14: 561–70.

Mesulam M. Slowly progressive aphasia without generalized dementia. Ann Neurol 1982; 11: 592–8.

Mesulam M. Primary progressive aphasia: a dementia of the language network. Dement Neuropsychol 2013; 7: 2–9.

Mesulam M, Wicklund A, Johnson N, Rogalski E, Léger GC, Rademaker A, et al. Alzheimer and frontotemporal pathology in subsets of primary progressive aphasia. Ann Neurol 2008; 63: 709–19.

Nasreddine ZS, Phillips NA, Bedirian V, Charbonneau S, Whitehead V, Collin I, et al. The Montreal Cognitive Assessment, MoCA: a brief screening tool for mild cognitive impairment. J Am Geriatr Soc 2005; 53: 695–9.

Oba H, Yagishita A, Terada H, Barkovich A, Kutomi K, Yamauchi T, et al. New and reliable MRI diagnosis for progressive supranuclear palsy. Neurology 2005; 64: 2050–5.

Oishi K, Faria A, Jiang H, Li X, Akhter K, Zhang J, et al. Atlas-based whole brain white matter analysis using large deformation diffeomorphic metric mapping: application to normal elderly and Alzheimer's disease participants. Neuroimage 2009; 46: 486–99.

Paviour D, Price S, Stevens J, Lees A, Fox N. Quantitative MRI measurement of superior cerebellar peduncle in progressive supranuclear palsy. Neurology 2005; 64: 675–9.

Peelle JE, Troiani V, Gee J, Moore P, McMillan C, Vesely L, et al. Sentence comprehension and voxel-based morphometry in progressive nonfluent aphasia, semantic dementia, and nonaphasic frontotemporal dementia. J Neurolinguistics 2008; 21: 418–32.

Petersen RC, Roberts RO, Knopman DS, Geda YE, Cha R, Pankratz V, et al. Prevalence of mild cognitive impairment is higher in men the mayo clinic study of aging. Neurology 2010; 75: 889–97.

Pramstaller PP, Marsden CD. The basal ganglia and apraxia. Brain 1996; 119 (Pt 1): 319–40.

Roberts RO, Geda YE, Knopman DS, Cha RH, Pankratz VS, Boeve BF, et al. The Mayo Clinic Study of Aging: design and sampling, participation, baseline measures and sample characteristics. Neuroepidemiology 2008; 30: 58–69.

Rogalski E, Cobia D, Harrison TM, Wieneke C, Weintraub S, Mesulam MM. Progression of language decline and cortical atrophy in subtypes of primary progressive aphasia. Neurology 2011; 76: 1804–10.

Rogalski E, Cobia D, Martersteck A, Rademaker A, Wieneke C, Weintraub S, et al. Asymmetry of cortical decline in subtypes of primary progressive aphasia. Neurology 2014; 83: 1184–91.

Rogalsky C, Hickok G. The role of Broca's area in sentence comprehension. J Cogn Neurosci 2011; 23: 1664–80.

Rohrer JD, Rossor MN, Warren JD. Apraxia in progressive nonfluent aphasia. J Neurol 2010; 257: 569–74.

Song SK, Sun SW, Ju WK, Lin SJ, Cross AH, Neufeld AH. Diffusion tensor imaging detects and differentiates axon and myelin degeneration in mouse optic nerve after retinal ischemia. Neuroimage 2003; 20: 1714–22.

Strand EA, Duffy JR, Clark HM, Josephs K. The apraxia of speech rating scale: a tool for diagnosis and description of apraxia of speech. J Commun Disord 2014; 51: 43–50.

Team R. RStudio: integrated development for R. Boston, MA: RStudio, Inc.; 2015.

Tsuboi Y, Slowinski J, Josephs KA, Honer WG, Wszolek ZK, Dickson DW. Atrophy of superior cerebellar peduncle in progressive supranuclear palsy. Neurology 2003; 60: 1766–9.

Tzourio-Mazoyer N, Landeau B, Papathanassiou D, Crivello F, Etard O, Delcroix N, et al. Automated anatomical labeling of activations in SPM using a macroscopic anatomical parcellation of the MNI MRI single-subject brain. Neuroimage 2002; 15: 273–89.

Vemuri P, Whitwell JL, Kantarci K, Josephs KA, Parisi JE, Shiung MS, et al. Antemortem MRI based STructural Abnormality iNDex (STAND)-scores correlate with postmortem Braak neurofibrillary tangle stage. Neuroimage 2008; 42: 559–67.

Weintraub S, Mesulam MM, Wieneke C, Rademaker A, Rogalski EJ, Thompson CK. The northwestern anagram test: measuring sentence production in primary progressive aphasia. Am J Alzheimers Dis Other Demen 2009; 24: 408–16.

Whitwell JL, Avula R, Senjem M, Kantarci K, Weigand S, Samikoglu A, et al. Gray and white matter water diffusion in the syndromic variants of frontotemporal dementia. Neurology 2010; 74: 1279–87.

Whitwell JL, Duffy JR, Machulda MM, Clark HM, Strand EA, Senjem ML, et al. Tracking the development of agrammatic aphasia: a Tensor-Based Morphometry Study. Cortex 2017; 90: 138–48.

Whitwell JL, Duffy JR, Strand EA, Xia R, Mandrekar J, Machulda MM, et al. Distinct regional anatomic and functional correlates of neurodegenerative apraxia of speech and aphasia: an MRI and FDG-PET study. Brain Lang 2013a; 125: 245–52.

Whitwell JL, Jack C, Parisi JE, Gunter JL, Weigand SD, Boeve BF, et al. Midbrain atrophy is not a biomarker of progressive supranuclear palsy pathology. Eur J Neurol 2013b; 20: 1417–22.

Whitwell JL, Jones DT, Duffy JR, Strand EA, Machulda MM, Przybelski SA, et al. Working memory and language network dysfunctions in logopenic aphasia: a task-free fMRI comparison with Alzheimer's dementia. Neurobiol Aging 2015; 36: 1245–52.

Whitwell JL, Master AV, Avula R, Kantarci K, Eggers SD, Edmonson HA, et al. Clinical correlates of white matter tract degeneration in progressive supranuclear palsy. Arch Neurol 2011; 68: 753–60.

Whitwell JL, Schwarz CG, Reid RI, Kantarci K, Jack CR, Josephs KA. Diffusion tensor imaging comparison of progressive supranuclear palsy and corticobasal syndromes. Parkinsonism Relat Disord 2014; 20: 493–8.

Yorkston K, Strand E, Miller R, Hillel A, Smith K. Speech deterioration in amyotrophic lateral sclerosis: implications for the timing of intervention. J Med Speech Lang Pathol 1993; 1: 35–46.

Yushkevich PA, Avants BB, Das SR, Pluta J, Altinay M, Craige C, et al. Bias in estimation of hippocampal atrophy using deformation-based morphometry arises from asymmetric global normalization: an illustration in ADNI 3 T MRI data. Neuroimage 2010; 50: 434–45.